AGU PUBLICATIONS

JGR

Journal of Geophysical Research: Solid Earth

RESEARCH ARTICLE
10.1002/2017JB014117

Key Points:
- Rigorous paleoseismic record of the last glacial Lake Lisan based on three sites is presented
- The Lisan Formation at the deep lake is 3 times thicker than at margins due to mass transport deposits
- Lake margin and deep-lake deformations and MTDs together present basin-wide earthquake and mass transport record

Supporting Information:
- Supporting Information S1

Correspondence to:
E. Kagan,
elisa.kagan@mail.huji.ac.il

Citation:
Kagan, E., Stein, M., & Marco, S. (2018). Integrated paleoseismic chronology of the last glacial Lake Lisan: From lake margin seismites to deep-lake mass transport deposits. *Journal of Geophysical Research: Solid Earth*, *123*, 2806–2824. https://doi.org/10.1002/2017JB014117

Received 2 MAR 2017
Accepted 29 DEC 2017
Accepted article online 22 JAN 2018
Published online 6 APR 2018

Integrated Paleoseismic Chronology of the Last Glacial Lake Lisan: From Lake Margin Seismites to Deep-Lake Mass Transport Deposits

Elisa Kagan[1,2], Mordechai Stein[1,3], and Shmuel Marco[2]

[1]Geological Survey of Israel, Jerusalem, Israel, [2]Department of Geophysics, Tel Aviv University, Tel Aviv, Israel, [3]Institute of Earth Sciences, Hebrew University of Jerusalem, Givat Ram, Israel

Abstract Seismically disturbed sedimentary sequences (seismites) in the last glacial (70–14 ka) Lisan Formation are exposed in the marginal terraces of the Dead Sea and recovered from sedimentary core drilled by the International Continental Scientific Drilling Programs at the depocenter of the lake at water depth of 300 m. The core reveals various types of centimeter- to meter-scale disturbed lake sediments: turbidites, homogenites, slumps, and other deformations, interspersed with undisturbed lamination. The transported sediments comprise a main source of the thickness tripling of the Lisan Formation at the depocenter of the lake compared to the margins. Excluding (mass transport deposits MTDs) from chronology yields a normal, event-free age-depth model for core. Moreover, time intervals of units missing at the exposed sections of the lake margin are synchronous with intervals of mass transport deposits (MTDs) at the deepest lake floors. In the deep core, the recurrence interval range of MTD with thickness $>$ 1 cm is ~ 100–300 years, while that of the thick MTD ($>$50 cm) is ~ 2,500 years, twice the recurrence interval of the seismites at the lake's margins. The ~1,000 year recurrence at the lake's margins lies within the ranges that have been calculated for ~*M*6.5–7 earthquakes. The significantly higher figure shown by depocenter core suggests activity on various faults and the response of the lake sediments in the entire Dead Sea basin. Overall, an unprecedented chronology of seismic activity was achieved for the late Pleistocene Lisan Formation providing a framework of earthquake activity in the vicinity of the Dead Sea basin during the period of the last high lake stand.

1. Introduction

The lacustrine formations exposed at the margins of the modern Dead Sea comprise a unique archive of late Quaternary environmental (climate and hydrology) and paleoseismic history (Marco et al., 1996; Neev & Emery, 1967; Stein, 2001, 2014). This stems from the high sedimentation rate (e.g., ~ 0.5–1 m/kyr), the annual mode of deposition of the sediments (e.g., the laminated sections of the Lisan Formation; see below), and the possibility to establish precise and high-resolution chronologies by U-Th dating of the primary aragonite or radiocarbon dating of organic debris (Haase-Schramm et al., 2004; Kagan et al., 2011; Ken-Tor et al., 2001; Schramm et al., 2000; Stein & Goldstein, 2006; Torfstein, Goldstein, Kagan, et al., 2013). Marco et al. (1996) combined sparse chronological data with detailed description of disturbed sedimentary layers in the last glacial (~ 70–14 ka) Lisan Formation exposed in the Perazim Valley and at the foothill of the Masada archeological fortress (Figure 1) to produce a first profile of temporal appearance of paleo-earthquakes during the Lisan time. These authors identified seismites in the Dead Sea lacustrine formations and outlined the observation of clustering of the earthquake events. Documentation of the seismites was later extended to the Holocene Ze'elim Formation (Kagan et al., 2011; Ken-Tor et al., 2001; Migowski et al., 2004). The chronology of breccia layers in the late Holocene lake-margin section demonstrates excellent agreement with historical earthquakes in the Dead Sea region, attesting to the validity of the identification of the breccia layers in the Dead Sea Formations as earthquake-induced structures—that is, seismites.

The exploration of the paleoseismic history of the late Quaternary Dead Sea basin (DSB) was accompanied by significant advances in establishing the stratigraphic-chronological framework of the Lisan Formation based on several exposed sections at the DSB (Torfstein, Goldstein, Kagan, et al., 2013) and the recent recovery of deep sedimentary cores at the abyssal (300 m water depth) and shallow floors of the modern Dead Sea (the Dead Sea International Continental Scientific Drilling Programs (ICDP) drilling project; Stein et al., 2011; Neugebauer et al., 2014, Torfstein et al., 2015). The detailed stratigraphy and improved chronology

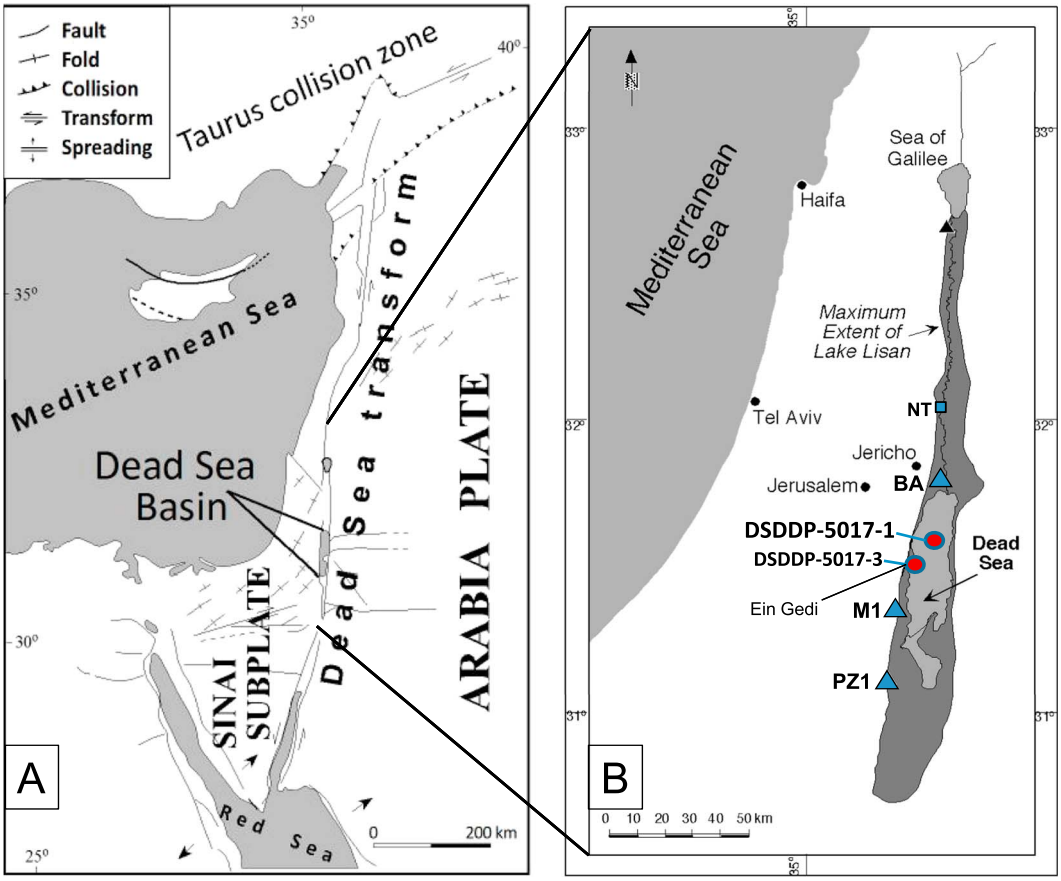

Figure 1. Location map. (a) Regional tectonics modified after Garfunkel (1981). (b) Study sites and locations mentioned in the paper; dark gray: maximum extent of Lake Lisan at Last Glacial Maximum, light gray: Dead Sea and Sea of Galilee.

of the Lisan Formation at the marginal terraces and deep floor of the lake allow us to establish a comprehensive integrated history of earthquake-induced sedimentary structures (seismites) at the entire DSB during the time interval of 70–14 ka. We accomplish here for the first time an integrated multisite seismic chronology at the marginal terraces and describe the appearance and chronology of mass transport deposits (MTDs) at the abyssal plains of Dead Sea and relate their formation to earthquake triggering. Overall, we present a comprehensive chronology and recurrence intervals of earthquakes in the last glacial DSB.

Sediment sequences containing MTDs have widely been used successfully for paleoseismic studies. Recently, for example, this approach has been applied effectively in the Cascadia region (Adams, 1996; Goldfinger et al., 2007; Goldfinger et al., 2003; Morey et al., 2013), France (Chapron et al., 1999; Wilhelm et al., 2016), British Columbia, Canada (Blais-Stevens & Clague, 2001), Switzerland (Schnellmann et al., 2006; Strasser et al., 2013), Chile (Blumberg et al., 2008; Moernaut et al., 2014), and Turkey (Avşar et al., 2016; Schwab et al., 2009). Earthquake triggering for mass transport at Lake Lisan (paleo-Dead Sea) is supported by its location on the seismically active Dead Sea Transform (DST) and by the on-shore association of deformations associated with faulting (Marco & Agnon, 2005).

2. Geology, Tectonics, and Seismicity in the Region

The DSB is located along the DST (Figure 1), which extends from the Red Sea in the south to the North Anatolian Fault in the north and defines the boundary between the Sinai subplate and the Arabian plate. The fault, comprising mainly N-S striking left-lateral transform with normal faulting along its margins and thrusting at northeast striking bends, has been active since the Neogene time (cf. Freund et al., 1968; Garfunkel, 1981). GPS measurements along the fault yield modern slip rate estimates of ~4–4.9 mm/yr (Le Beon et al., 2008; Masson et al., 2015). This value is intermediate in the estimated range of slip rates (1.5–8.5 mm/yr) calculated by various workers using geological and archeological evidence of offset (reviewed in Marco & Klinger, 2014).

Frequent seismic activity along the DST has been detected in the past century (Salamon et al., 2003) and was recorded historically and archeologically over the past 4,000 years (e.g., Ambraseys, 2009; Ben-Menahem, 1991). The correlation between the historically and archeologically documented earthquakes and the nearby lake archives allows the assessment of the validity of the lake sediment chronology as well as the interpretation of the disturbed sedimentary layers as true seismites. This correlation allows constraining seismic intensity thresholds for seismites (Agnon, 2014; Kagan et al., 2011; Migowski et al., 2004), which can be used to determine the strength of prehistoric earthquakes.

3. Paleoseismic Records in the Exposed Lacustrine Sediments, DSB

The disturbed sedimentary sequences in the Lisan Formation (Figure 2) were described as intraclast breccias, interpreted as earthquake-induced structures—*seismites* (Agnon et al., 2006, and references therein). This interpretation was based on the association of the disturbed layers with surface ruptures, mainly synsedimentary normal faults (Marco & Agnon, 1995; Marco et al., 1996). Marco et al. (1996) also identified sedimentary structures such as liquefaction in sands or diapirs that characterize earthquake-induced structures in the lacustrine environment. By comparison with recent earthquake surface ruptures, they assumed that these seismites were triggered by $M > 5.5$ earthquakes (McCalpin, 2009). Other types of seismites in the form of slump sheets that are exposed in the Perazim Valley exhibit fold-and-thrust structures. Basin-wide structural analyses show transport toward the depocenter and evidence for seiche waves (Alsop & Marco, 2011, 2012a, 2012b, 2014). Post-Lisan, most of the historically recorded earthquakes in the area could be matched to the disturbed layers (seismites) identified and (radiocarbon) dated in the exposures of the Holocene Ze'elim Formation. This comparison verified the identification of the disturbed lacustrine sedimentary sequences as earthquake-induced disturbances (Ken-Tor et al., 2001; Migowski et al., 2004). Moreover, the work on the Ze'elim Formation revealed that various sites in the lake recorded a somewhat different pattern of historical earthquakes (Kagan et al., 2011); thus, a complete picture of the regional seismic activity can be achieved only by integration of several sedimentary records from various sites in the DSB.

4. Paleoseismic Chronology From Outcrops of the Lisan Formation, New and Revisited

Until recently, the chronology of the seismic events in the lacustrine archives of the Dead Sea was based on U-Th ages of primary aragonite from the Perazim Valley (PZ1 section) and the Masada M1 section (e.g., Marco et al., 1996). Based on these data, Marco et al. (1996) suggested temporal clustering of the paleoseismic events, where ~10 kyr of seismic activity alternated with ~10 kyr of quiescence. Yet when more data were obtained to construct the age-height model of the PZ1 section (Haase-Schramm et al., 2004; Schramm et al., 2000), it was realized that the scenario is more complex (Stein, 2011). The age-height model of the PZ1 section (Haase-Schramm et al., 2004) shows that the section includes two hiatuses (~67–62 ka and 49–43.5 ka). The site also contains several intervals of gypsum, which are stiffer than the sequences of alternating aragonite silty-detritus laminae (the *aad* facies, see Machlus et al., 2000) and less likely to deform during earthquake shaking. The only interval of continuous sedimentation of *aad facies* is the Upper Member of the Lisan Formation (or the "White Cliff") deposited between ~31 and 17 ka, when the lake reached its highest stands (~200 to ~170 m below mean sea level) (Bartov et al., 2003). During this time interval nine seismites were recorded, yielding a mean recurrence time of ~1,500 years.

The Lisan marginal sections discussed here are ~25–40 m thick. The variations in formation thickness in the marginal terraces reflect proximity of lake's margins at time of deposition (e.g., presence of sands and thicker detritus units at Perazim PZ1 section that lies ~70 m higher on the pre-Lisan relief compared to Masada and Beit Ha'Arava, Bartov et al., 2007; Waldmann et al., 2007). The Haase-Schramm et al. (2004) chronology of the PZ1 section was extended by Torfstein, Goldstein, Kagan, et al. (2013) to other stratigraphic sections in the DSB-Jordan Valley including the Masada (M1) and the Beit Ha'Arava (BA) and the Tovlan sections (locations in Figure 1). Torfstein, Goldstein, Kagan, et al. (2013) integrated the U-Th age models from all these sections, combined them with the Haase-Schramm PZ1 age model, and used anchor ages of major gypsum units that appear in all sections to produce a "multisite" integrated chronology of the Lisan Formation. This unprecedented chronology allows us to reexamine the temporal and spatial patterns of earthquake-triggered sedimentary disturbances (seismites) in the Lisan Formation. Moreover, the various sections complement

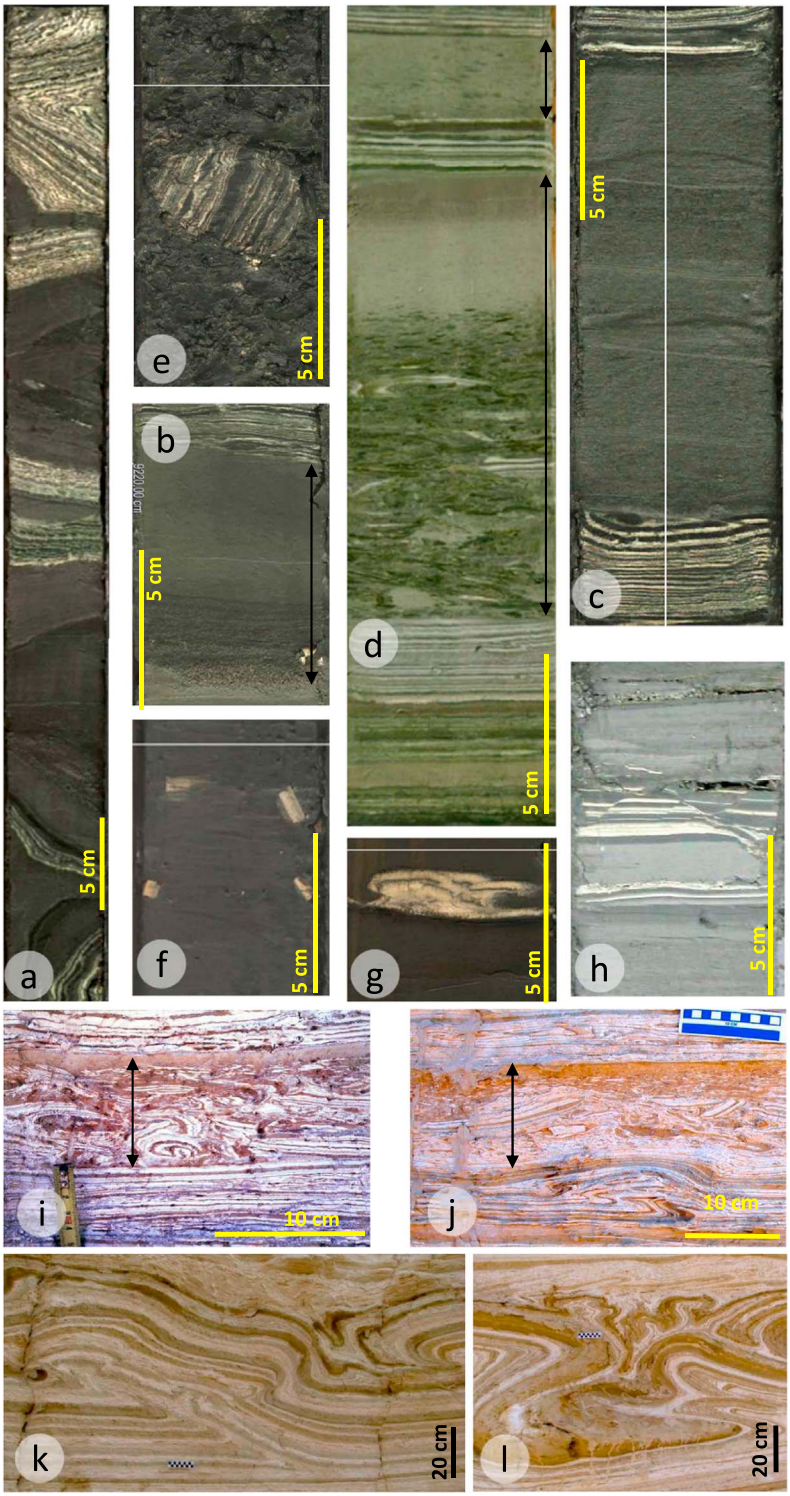

Figure 2. Examples of MTDs and otherwise deformed sediments (a–g) in the Lisan Formation of the 5017-1 core and (h–j) from the western lake margin. Depocenter facies (core): *Major slump:* (a) (~117 meters below lake floor (mblf)) large-scale folded beds, with horizontal fold hinges. *Debrites/turbidites:* (b) (92.2 mblf) nonlaminated clay to silt-sized detritus with coarse grains near base (event unit indicated by arrow); (c) (~166.4 mblf) nonlaminated clay to silt-sized detritus with erosion of underlying laminae; (d) (~107.7 mblf): intraclast breccia above base, mostly upward fining, clay to silt-sized detritus, dark fine cap (lower arrow); (e) (~162 mblf) debrite mud with large clast of laminated sediment. (f) *Breccia* **(~**40 mblf, post-Lisan**)**: broken fragments of aragonite laminae in dark matrix; breccia unit also indicated by upper arrow in "c." (g) *Small fold* (~26.2 mblf; post-Lisan depth). (h) *Faulted laminae*: laminae with small normal offsets (~1 cm). Lake margin facies (outcrop): (i and j) *breccia* (indicated by arrows), composed of upward fining *intraclast* fragments of laminae (Masada, MA, site). (k and l) *Folded strata* showing tripling of original thickness (interpreted as short transport slump sheet at the lake margin flat shelf by Alsop & Marco, 2011).

each other allowing the reconstruction of a continuous (undisturbed by sedimentary hiatuses) paleoseismic record for the time interval of ~70–14 ka in the DSB. For example, at the M1 section the new age-height model (Torfstein, Goldstein, Kagan, et al., 2013) reveals a significant unconformity between 40 and 31 ka, below the White Cliff. Yet, other parts of the M1 section are more continuous and can complement missing parts in the PZ1 section (Table 1 and Figure 3a). The Tovlan section (NT, Figure 1) located at the central Jordan Valley is dominated by fluvial deposits and contains only one significant seismite and is excluded from the multisite paleoseismic comparison. The most complete sections of the marginal Lisan Formations sites are the Upper Member White Cliff spanning 31 to ~17 ka at Masada M1 section (8.8 m) and Perazim valley PZ1 section (6 m). At Beit Ha'Arava the White Cliff is only 5 m in thickness and the ages are less certain. Thus, for considerations of recurrence interval the White Cliff at Beit Ha'Arava is excluded. However, the sequences deposited at Beit Ha'Arava between ~70 and 58.5 ka (Lower Member) and 47.5 to 40 ka (between the Curled and Broken Gypsum Unit, Figure 3a) that are continuous and comprise *aad* sequences can be considered for recurrence intervals calculation.

The main observations from the multisite exposures comparison are as follows:

1. The thickness of the exposed sections of the Lisan Formation studied here varies between 23 and 38 m. The number of seismites at each specific site varies from 21 to 25, accounting for 5–10% of the sections' thicknesses. In detail, the Perazim section is 38 m thick, including 29 seismites, which are ~10% of the section thickness; the Masada section is 29 m thick, including 21 seismites, which make up ~5% of the section thickness; and the Beit Ha'Arava section is 23 m thick and has 35 seismites, which are ~10% of the section thickness.
2. The missing sedimentary intervals (hiatuses) in the PZ1 and M1 sections (~49–43.5 and ~40–30 ka, respectively) appear in other sections, and thus it is possible to complement the apparently missing seismites. For example, the ~40–31 ka hiatus in M1 that was previously explained by transgressional erosion upon the subsequent rise of the lake to its high Marine Isotope Stage 2 (MIS2) (~ 29–17.4 ka) stand (see Bartov et al., 2007; Torfstein, Goldstein, Stein, et al., 2013), as well as a shorter but significant hiatus at BA, can be correlated to the existing sections at PZ1. Interestingly, this time interval also shows three very thick MTDs in the deep-lake core (see section 8). The ~49–43.5 ka hiatus at PZ1 that was related to lake retreat (Machlus et al., 2000) can be complemented by synchronous units in the M1 and BA sections. In this way Figure 3 (and Table 1) presents an integrated picture of seismite occurrence throughout the Lisan Formation in the DSB.
3. Recurrence intervals of seismites (n = number of seismites) and coefficient of variation (CoV) at the marginal outcrops during intervals when no hiatuses disturbed the stratigraphic unit are as follows: Masada (M1 section) Upper Member (30–17.1 ka) (n = 11): Recurrence interval (RI) = average 1.2 kyr and CoV = 0.6; Perazim (PZ1 section) Upper Member (n = 9): RI = average 1.5 kyr and CoV = 0.7; Beit Ha'Arava (B1 section) Lower Member (69–59 ka) (n = 10) RI = average 1.0 kyr; Beit Ha'Arava (B1 section) Middle Member (48–40 ka) (n = 8) RI = average 1.0 kyr. Coefficients of variation (see Kagan & Jackson, 1991) denote no clear clustering of earthquakes within each of these intervals. However, the seismite distribution in the entire Lisan section does show clustering. The clusters are on the order of length of the whole white cliff, therefore they can only be discerned by looking at the entire section. We argue here that only by recording large time windows can we discern clusters. Considering all seismites in an integrated section for the Lisan Formation, we count a minimum 49 seismites and calculate an average integrated recurrence interval of ~1,100 years. This value is the same as the RI shown by the Upper Member at the M1 Masada section, which is the best documented and dated segment of the Lisan Formation. It can be therefore argued that the RI of 1,100 years is the "typical recurrence interval" of the Lisan Formation at the marginal terraces. The number of 49 seismites represents a minimum number of earthquakes and a maximum recurrence time interval since it is possible that the missing sections have a higher number of seismites than the contemporaneous existing sections, and also it is possible that within specific intervals apparently contemporaneous seismites recorded in various sections are not the results of the same earthquakes.

5. The Depocenter Core and MTDs

5.1. The Deep-Lake ICDP-DSDDP Core

The ICDP drilling project at the Dead Sea was conducted between November 2010 and March 2011 by the nonprofit corporation Drilling, Observation and Sampling of the Earth's Continental Crust team (Stein et al.,

Journal of Geophysical Research: Solid Earth

10.1002/2017JB014117

Table 1

Age Data for Lisan Formation for Seismites From Three Outcropping Sections: Perazim Valley (PZ1), Masada Fortress (M1), and Beit Ha'Arava (BA), and for MTDs From the DSDDP-5017-1-A Core

		Masada M1 Seismites				Perazim PZ1 Seismites				Beit Ha'Arava Seismites				5017-1-A Core MTDs			
Age (kyr)	Stratigraphic marker	Height (cm)	Thickness (cm)	Age (kyr)	Sedimentation rate	Height (cm)	Thickness (cm)	Age (kyr)	Sedimentation rate	Height (cm)	Thickness (cm)	Age (kyr)	Sedimentation rate	Depth below lake floor (m), top	MTD type	Thickness (cm)	Age (ka)
														88.5	D	60	~10.8
														90.1	D	50	12.0
14.5	**Section top**	**2,930–2,970**		**14.5**		**3,785**		**14.5**		**2,285**		**14.5**					
										2,229	1.2	15.0					
					1.2 m/kyr	3,762	12	16.0	**0.5 m/kyr**	2,184	9	15.4	**1.1 m/kyr**	95.8	D	60	15.9
		2,650	32														
15.5–17.1	**"Upper gypsum" (UG)**	**2,623–2,813**		**15.5–17.1**		**3,661–3,736**		**15.5–17.1**		**2,178**	**Top of UG**	**15.5**		**101–99 m**			
		2,575	2	17.8		3,612	5	18.0		2,174	15	15.5					
		2,468	1	19.4		3,594	7	18.3		2,138	2.5	15.9					
										2,128	5.5	16.0					
		2,356	2	21.1		3,455	12	20.9		2,083	4	16.4		101	D	110	18.1
		2,301	2	22.0		3,374	2	22.3		2,056	2	16.7		102.1	S	110	18.1
		2,248	4	22.8		3,369	15	22.4		2,043	1.2	16.8					
		2,194	3	23.6	**0.8 m/kyr**	3,347	7	22.8	**0.6 m/kyr**	2,024	1	17.0		108.3	S	60	20.4
										1,973	**Base of UG**	**17.1**					
		1,997	2	26.6		3,204	15	25.4			***Hiatus***			111.6	S	60	24.4
		1,943	2	27.4		3,105	10	27.3		1,963	2	23.9					
		1,887	2	28.2						1,957	3	24.2	**0.22 m/kyr**	114.9	D	120	28.6
		1,828	3	29.1		2,909	15	30.8		1,853	10	28.9		117	S	790	29.5
		1,763	3	30.1													
31	**Base of White Cliff**	**1,705**		**31**		**2,900**		**31**		**1,788**		**31.8**					
						2,515	20	34.9						126	S	300	32.4
				~39.7–30 ka no sediments		**2,297–2,405**	**Clastics**	**37.1**						130.3	D	170	34.7
						2,142	6	38.7	**0.9 m/kyr**	**1,633–1,788**	**Hiatus**	**~38–32 ka**					
						2,114	16	39.0		1,678	8	?		132.8	S	470	36.3
						2,073	27	39.4		1,611	3	~39					
39.7	**"Broken gypsum"**	**1,690**		**39.7**		**2,046–2,142**	**Clastics**	**39.7**		**1,420–1,493**		**39.7**					
										1,400	1	40.2					
										1,396	1	40.3					
						1,943	37	41.2		1,365	2	41.1					
		1,586	2	41.6		1,810	10	43.2		1,357	0.8	41.3					
		1,528	2	42.6	**0.6 m/kyr**	1,781.0	8	43.5	**0.7 m/kyr**	1,290	1	42.9	**0.4 m/kyr**				
		1,480	1	43.5						1,227	?	44.4					
										1,209	2	44.9					
								49–43.5 ka, no sediments		1,183	10	45.5					

Table 1. *(continued)*

		Masada M1 Seismites				Perazim PZ1 Seismites				Beit Ha'Arava Seismites				5017-1-A Core MTDs			
Age (kyr)	Stratigraphic marker	Height (cm)	Thickness (cm)	Age (kyr)	Sedimentation rate	Height (cm)	Thickness (cm)	Age (kyr)	Sedimentation rate	Height (cm)	Thickness (cm)	Age (kyr)	Sedimentation rate	Depth below lake floor (m), top	MTD type	Thickness (cm)	Age (ka)
47.5–49.0	**"Curled gypsum"**	**1,236–1,255**		**47.5–49.0**		**1,770**	**Sand 6 cm + hiatus**			**1,047–1,103**		**47.5–49.0**					
						1,745	16	49.1						145.3	D	50	49.0
						1,602	12	49.9						146.5	D	320	49.9
						1,564	17	50.1						149.7	D	420	49.9
		1,115	80	50.5		1,511	36	50.4									
						1,339	3	51.3						155.5	D	170	51.9
					0.8 m/kyr	1,320	3	51.4	**1.7 m/kyr**					157.2	D	70	51.9
						1,294	15	51.5									
						1,260	14	51.7									
						1,220	48	51.9									
						1,115	20	52.5									
						1,074	10	52.7						160.7	D	60	55.5
		842	5	53.8		1,060	50	53.1						161.4	D	70	55.6
54.0–56.0	**"Small gypsums"**	**685–825**		**54.0–56.0**		**829–908**		**54.0–56.0**		**800–837**		**54.0–56.0**					
		775	8	54.1													
		685	3	56.0	**0.5 m/kyr**				**1.5 m/kyr**	738	15	56.8	**0.79 m/kyr**				
		682	53	56.1						622	1	58.3					
		580	2	58.2						619	1	58.3					
58.5–61.0	**"Lower gypsum"**	**418–565**		**58.5–61.0**		**338–465**		**58.5–61.0**		**507–603**		**58.5–61.0**					
										337	3	63.9					
		387	2	61.6						281	8	64.8		168.3	D	80	63.6
										263	8	65.1					
										173	18	66.6					
										150	27	67.0					
					0.5 m/kyr					110	17	67.7	**0.6 m/kyr**				
							Hiatus	**68–62**		90	4	68.0					
										78	9	68.2					
						34	9	68.4		65	30	68.4					
		22	5	69.1						43	14	68.8					
69.5	**Lisan base at outcrops**	**0**		**69.5**		**0**		**69.5**		0		**69.5**		**178.6**			
														179.5	D	60	75.9
														181.4	D	320	77.3
														190.2	D	70	83.3
														191.4	D	60	83.9
														194	D	70	85.7
														195.3	D	50	86.0
														198.3	D	50	87.0
Lithology-determined base of Lisan Fm. in core														**199.2**			

Note. Dark gray rows indicate stratigraphic markers and their anchor ages from the outcrops (Torfstein, Goldstein, Kagan, et al., 2013). Light gray rows indicate, as marked, hiatuses and specific sedimentary units (this study and after Torfstein, Goldstein, Kagan, et al., 2013). Uncolored rows are laminated sediments (blank), seismites, or MTDs. Dates for the outcrop seismites are interpolated from the anchor ages, with uncertainties of 1,000 to 2,000 years (at the Lisan top and base, respectively), based on 95% confidence limit of Bayesian height models (see Torfstein, Goldstein, Kagan, et al., 2013), while for the densely dated PZ1 section the age-height model has an error of only 800 years (Haase-Schramm et al., 2004). Dates for the MTDs are calculated by the *event-free model* in this study (see text and Table 2). Uncertainty in the core event-free age-depth model is estimated at approximately ~2 kyr throughout the Lisan period. Data for stratigraphic markers and for hiatuses in bold.

AGU Journal of Geophysical Research: Solid Earth 10.1002/2017JB014117

2011). Ten cores were recovered, four from the shallow lake near the Ein Gedi Spa shore (Site 5017-3, 31°25′22.74″N, 35°23′39.58″E, lake floor at drill site ~ −426 m above mean sea level (amsl), 2.3 m water depth) and six at the lake's depocenter (Site 5017-1 (31°30′28.98″N, 35°28′15.60″E, lake floor at drill site ~ −725 m amsl, ~300 m water depth) (Figure 1). The cores were described and photographed in the field and at the GFZ-Potsdam core laboratory according to the ICDP protocol. Details of the coring campaign and core handling can be found in Neugebauer et al. (2014). The ICDP Dead Sea Deep Drilling Project (DSDDP) 5017-1-A core was split and visually inspected at the GFZ core laboratory. Additional analyses included optical line scanning, magnetic susceptibility analyses, and micro X-ray fluorescence (μXRF) element scanning (Neugebauer et al., 2014). The entire 455 m thick 5017-1-A core is described by Neugebauer et al. (2014) and comprises mainly units of marly facies (laminated detritus, laminated alternating aragonite and detritus, and laminated gypsum and detritus), salt, and MTDs (supporting information Figure S1). Here we focus on the deformed units in the interval of the Lisan Formation in the longest deep-lake core, DSDDP 5017-1-A, which are described and discussed for the first time in this paper. The core during this time interval shows 97% recovery. The new data are based on visual inspection at the GFZ core laboratory and examination of the deformed units using Corelyzer v2.0.1.

5.2. Lithology of the Lisan Formation Section in the DSDDP 5017-1-A Core

The Lisan Formation recovered in the DSDDP core comprises two main sedimentary units: laminated (undisturbed) units and transported/disturbed units (Figure S1). The laminated units include sequences of alternating laminae of primary aragonite and fine detritus similar to the *aad* facies that was described in the marginal terraces (Machlus et al., 2000), sequences of laminated fine detritus similar to the *ld* facies in the marginal terraces (Haliva-Cohen et al., 2012), and gypsum layers (up to 15 cm thick) (Neugebauer et al., 2014). The disturbed units include frequent convoluted and brecciated structures associated with MTDs. Salt units interlayered with muds appear below and above the Lisan Formation interval. In the DSDDP core 5017-1-A the thickness of the Lisan Formation is ~110 m, significantly higher than the formation thickness at the marginal terraces: ~25 m at Beit Ha'Arava; ~ 30 m at Masada, and ~ 40 m at Perazim Valley. The significant thickening of the Lisan Formation at the abyssal DSDDP site reflects mainly the effects of MTD and local slumps. This topic is elaborated on below.

5.3. MTD Structures in the Deep Core

We described and measured all laminated and nonlaminated sequences comprising the Lisan Formation interval in the deep core. The nonlaminated units in the deep core are brecciated (graded or not) and/or folded. These nonlaminated units range in thickness from ~0.01 up to 8 m. The general term given for these units here is MTDs. For the sake of simplicity, we use the term MTD in the broadest sense, that is, any form of movement of sediments; other authors may exclude turbidites and faulted strata from the term MTD (Mulder & Alexander, 2001).

Types of MTDs in the deep core are described here and in Figure 2: (1) *major slumps* (Figure 2a)—large-scale folded (with horizontal fold hinges) and fractured beds (up to ~8 m thick), often capped by dark breccia or homogenite; (2) *debrites: homogenite (*Figures 2b and 2c): erosional or nonerosional base, graded, usually upward fining, clay to silt-sized detritus, often looks homogeneous to the naked-eye, muds; (3) *turbidite* (Figures 2d and 2e): usually erosional base, coarse grain, or intraclast breccia above base, upward fining, often the middle part is homogeneous to the naked-eye, clay to silt-sized detritus, dark fine cap; (4) *brittle deformation: breccias* (Figure 2f): light or dark broken fragments of laminae in dark matrix; *microbreccia* (top of Figure 2d): submillimeter light and dark fragments in usually light gray matrix; (5) *ductile deformations* (Figure 2g) centimeter-scale folded aragonite and detritus laminae, horizontal fold hinges; (6) *discontinuous laminae*: packets of usually 5 to 10 laminae that are bounded laterally by quasi-homogenous detritus (minor amounts of these units); (7) *faulted laminae* (Figure 2h): laminae with small normal offsets (~1 cm) (minor amounts of these units).

We divide the MTDs into two main categories: slumps (lamination is mostly retained within the folds) and debrites (original lamination is destroyed during transport: homogenites, turbidites, and breccias). MTD or otherwise disturbed sediments comprise a major part of the Lisan section in the deep core. Of the 112 m of the Lisan Formation interval in the core (in between ~200 and 88 m core depth) 85 m (76%) are MTDs and 27 m (24%) are typical laminated *aad* (and some gypsum laminae) Lisan Formation sediments. MTDs 1–50 cm thick make up 42.5 m of the core, and MTDs of 50 cm and thicker comprise 42.5 m of the Lisan

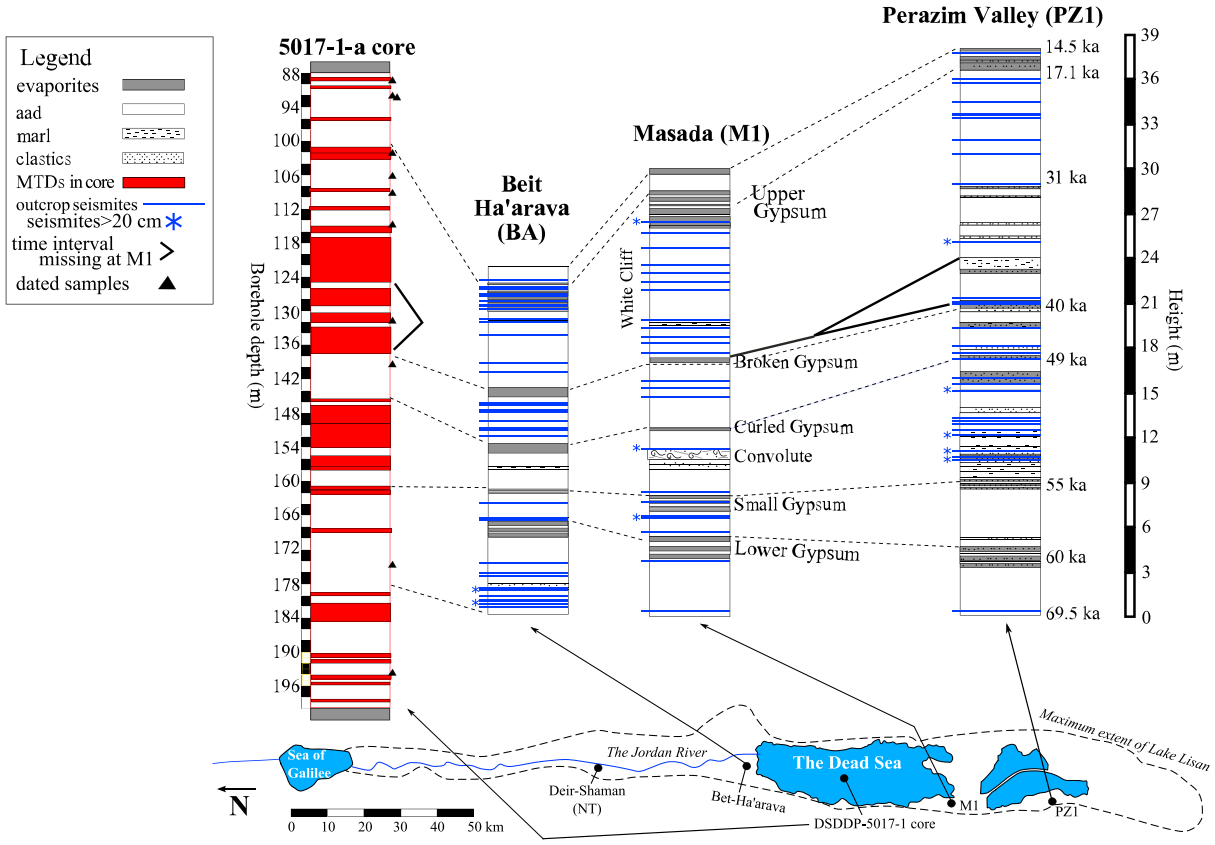

Figure 3. (a) Correlation of three Lisan Formation outcrop sections (Perazim PZ1, Masada M1, and Beit Ha'Arava BA), and the DSDDP-5017-1-A deep-lake core. Stratigraphic markers are correlated, aided by U-Th dating (Torfstein, Goldstein, Kagan, et al., 2013; Torfstein et al., 2015), radiocarbon dating (Kitagawa et al., 2017) (Table 1), and our event-free age model (Table 2). In the DSDDP core, presented in the leftmost column, MTDs >50 cm are marked (red bars, thickness is representative of MTD thickness in core). Additional core lithology is given in Figure S1. The seismites tops are marked in the outcropping lake margin sections marked (blue lines); thickness of blue lines is uniform, not representative of seismite thickness, and stars mark seismites >20 cm thick. Generalized lithology of PZ1 and M1 and map at bottom modified after Torfstein, Goldstein, Kagan, et al. (2013). (b) Temporal distribution of seismites in the three exposed sections (Masada (M1), Beit Ha'Arava (BA), and Perazim Valley (PZ1)) and MTDs from the DSDDP core hiatuses in the sections are marked (see Table 1 and text). Black vertical bar marks one occasion where thick MTDs coincide with missing sections in BA and M1 (see text for interpretation). For age uncertainties see Table 1 caption (not portrayed graphically here).

section in the core. Percentage (by thickness) of laminated sediment versus MTDs and other deformed sediments, distributed by depth, are shown in Figure 4. Percentages of MTD thickness were measured per core interval, the large majority of which have 100% core recovery (3.05 m thick). The MTDs are distributed throughout the Lisan Formation. However, very thick (>50 cm) MTDs are more common in the middle part (138–115 m) of the Lisan Formation section (Figure 3). The combined thickness of the laminated portions in the Lisan Formation in the core (29.3 m in entire Lisan Formation or 20.6 m for the 70–14 ka time interval, see section 6) is the same as the thickness of the laminated sediments at the lake margin sites (20–30 m). This is while the thickness of individual laminae of aragonite and silty detritus in the *aad* packages (millimeter scale) are approximately the same on average in both environments. This supports negligible deep-lake floor sediment removal.

5.4. Chronology of MTDs in the Core

The general age-depth model for the entire ~450 m long 5017-1-A core (Torfstein et al., 2015) was based on radiocarbon ages (top ~40 kyr), U-Th ages (measured on primary aragonite laminae), oxygen isotope matching to regional and global records (such as Heinrich events related gypsum units), and correlation of stratigraphic markers with well-dated on-shore counterparts. The Torfstein et al. (2015) age-depth model assumes a constant sedimentation rate (~1.7 m/kyr) for the Lisan interval (between 200 and 88 m core depth), a value that is 2 to 3 times higher than the sedimentation rate at the lake margin sites (e.g., PZ1

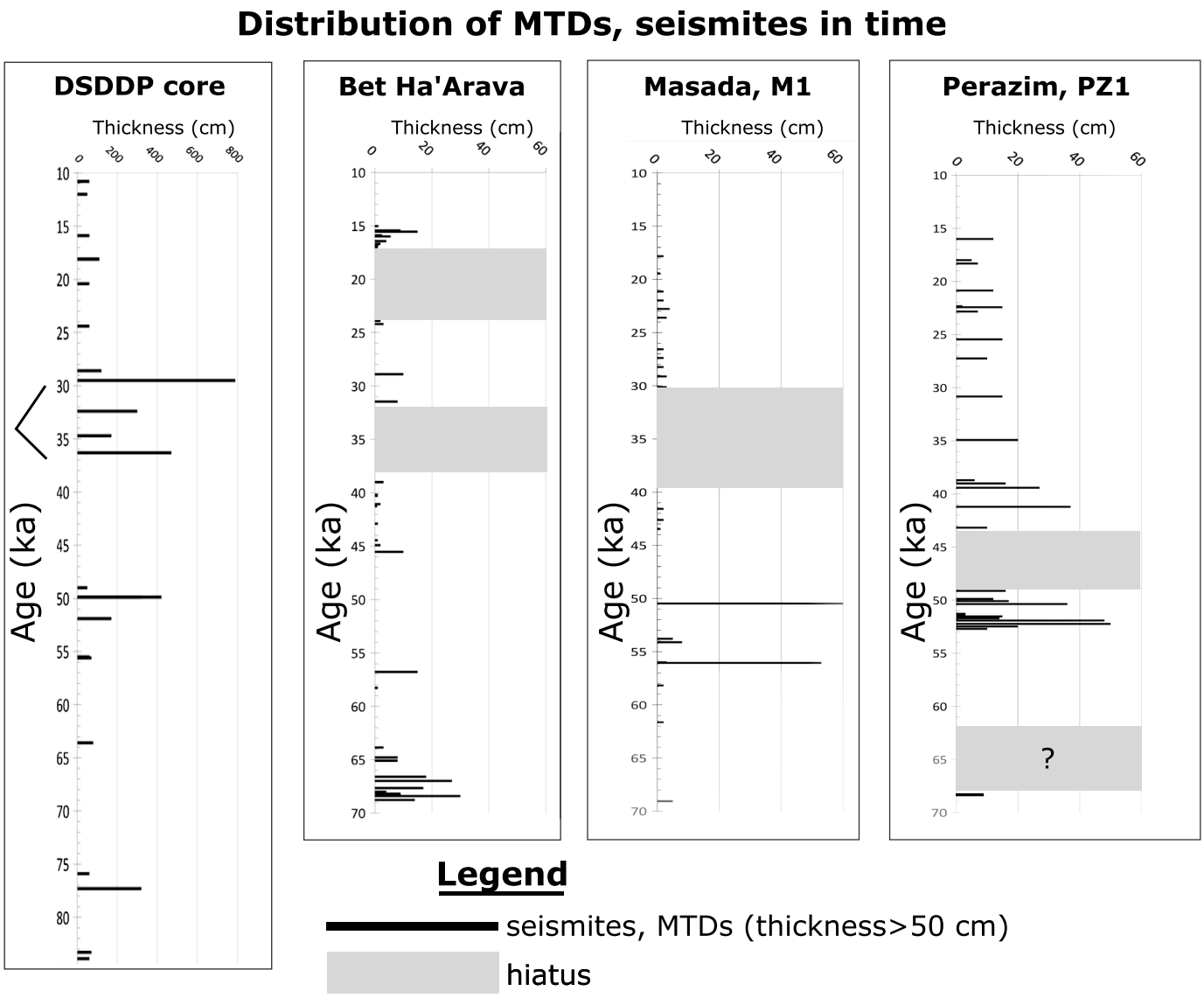

Figure 3. (continued)

~0.7 m/kyr, M1~0.8 m/kyr, Haase-Schramm et al., 2004; Torfstein, Goldstein, Kagan, et al., 2013). This large difference reflects the effects of the MTDs on the apparent sedimentation rate in the deep core since the major slumps and debrites (mass movement deposits) add considerable quantities of material essentially instantaneously ("events") to the core and must be taken into consideration in a more accurate age-depth model.

An "event-free" model is constructed here, removing from the section the >50 cm MTDs (Tables 2 and S1). The debrite thicknesses are considered here to be entirely added thickness to the section and are removed completely for the age model. The slumps on the other hand (six of them, see Table 1) probably include some original (in situ) laminae. Based on similar folded strata at the marginal terraces of the Lisan Formation (Alsop & Marco, 2011), we estimate that in folded slumps there is approximately a tripling of thickness, one-third original thickness, two-thirds addition to the section thickness. In some cases the slump is topped by debrite, and therefore each slump was individually examined and the amount of "additional thickness" was estimated. After constructing an event-free age-depth model, the MTDs are "returned" into the section (Figure 3a). Every core depth has a corresponding event-free depth (EFD), on which the age model is defined and the inferred ages of the MTDs is the age at their corresponding EFD (Table 2).

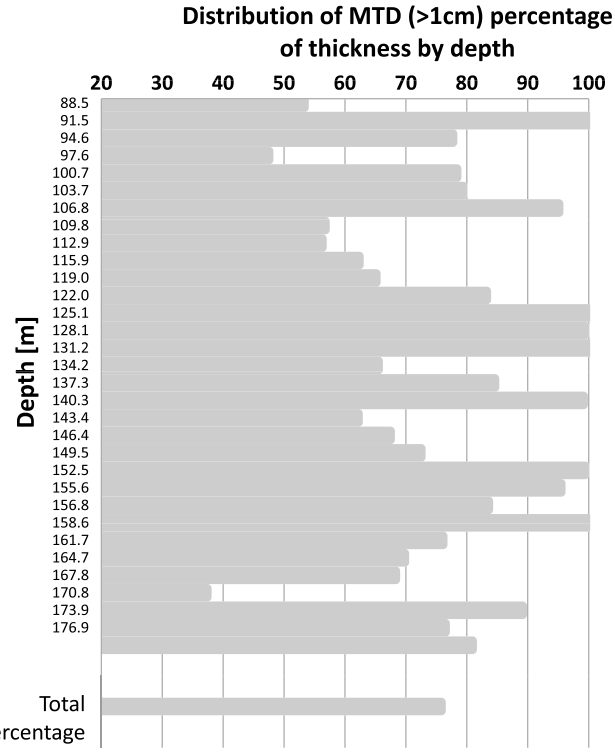

Figure 4. Percentage by thickness of all MTDs (>1 cm) versus laminated beds, with depth. Each bar represents the summation of the MTDs in a specific core interval (~3 m long), as a percentage.

5.5. Sedimentation Rate With or Without MTDs

The time interval of the Lisan Formation in the core (200–88 m core depth) spans ~69 kyr, from 83 to 14 ka. This time interval is longer than the time duration of the Lisan Formation at the marginal terraces (~ 70–14 ka, that corresponds to MIS4, MIS3, and MIS2 comprising the last glacial interval in the global chronology; see Haase-Schramm et al., 2004; Torfstein, Goldstein, Kagan, et al., 2013) and is based on the earlier appearance of the *aad* sequences in the lake depocenter and the evidence for freshening of the deepest brine already in the latest stages of MIS5 (e.g., Lazar et al., 2014; Levy et al., 2017; Neugebauer et al., 2016; Stein et al., 2017). This can be explained in several ways; however, in the absence of continuous exposure from shore to depocenter this would only be conjecture. The average sedimentation rate of the undisturbed laminated sequences (the *aad facies*) of the Lisan Formation at the deep core during the time interval of 83–14 ka is 0.43 m/kyr. This value is comparable to values calculated for the Lisan sections at the marginal terraces: 0.41 m/kyr at Beit Ha'Arava (BA) section, 0.53 m/kyr at the Masada M1 section, and 0.69 m/kyr at the Perazim PZ1 section (Haase-Schramm et al., 2004; Torfstein, Goldstein, Kagan, et al., 2013). We note above that ~10–30% of the slumps in the deep core possibly comprise original sequences of the Lisan Formation at the site of the deep core. This is because the major slumps could not be transported from a distance (the slumps would be destroyed) and they rather represent on-site deformation. Thus, the more event-free sedimentation rate in the abyssal plain could be higher than 0.43 m/kyr and could approach the value of the Masada section.

6. Comparison of Deformed Units in Lake Margin Sites and Deep Core

A multisite correlation of the Lisan outcrops at the marginal terraces was presented by Torfstein, Goldstein, Kagan, et al. (2013). This correlation was based on U-Th dating of aragonite samples near main gypsum units and other significant stratigraphic units that were used as stratigraphic "anchor units." From the age-height diagrams of Torfstein, Goldstein, Kagan, et al. (2013) we interpolate ages for the seismites in each outcrop sections (Table 1). We then correlated the seismites or seismites groups based on these ages and stratigraphic considerations (namely, major stratigraphic units such as prominent gypsum layers). Interpolation of MTD ages is discussed in section 5.4 above. The thickest MTDs, 50 cm and thicker, are presented in Figure 3 and correlated with groups of events in the lake margin sections (see Table 1). Age uncertainties are not portrayed graphically in Figure 3b.

The main observations from the comparison of the appearance of disturbed sedimentary structures (seismites) in the lake depocenter and the marginal terraces are as follows:

1. Considering age uncertainty of several hundred years that was calculated for the multisite chronology (Torfstein, Goldstein, Kagan, et al., 2013), most of the seismites that were identified in the marginal terraces can be broadly chronologically correlated to the depocenter.
2. Pronounced seismites in the marginal terraces appear as significant slumps in the depocenter, for example, the convolute unit at Masada (supporting information Figure S1) is correlated with a ~ 4 m slump in the depocenter.
3. The sedimentary gaps in the seismite records of the individual marginal terraces are filled when all the studied sections are considered, and the data are integrated (as describe above). The record of the deep core also fills these gaps. Two prominent examples are the following: (1) the interval of the ~ 49–43.5 kyr hiatus at the PZ1, Perazim Valley section, coincides with a 3 m thick slump in the deep core; (2) the interval of the ~40–30 ka hiatus at the M1 Masada section and the BA section hiatus (38–32 ka) coincides with very thick MTDs, including ~8 m thick slump at the deep core (considering age uncertainties). We propose the possibility that the same seismic events caused slumping and removal of sediments in the marginal sites

Table 2
Event-Free Age Model Is Presented Here With the Estimated Added Thickness of the MTDs (>0.5 m) Removed From the Section

	Thickness of added material (m)	Sum of added event thickness above (m)	Added material top, core depth (m)	Added material bottom, core depth (m)[b]	EFD (top) (m)	Dated horizons age (ka)	Event-free model ages (ka)	Event-free sedimentation rate (m/kyr)
MTD-1	**0.6**	**0**	**88.5**	**89.1**	**88.5**		**~10.8**	
Date (C14 cal)		0.6	89.25		88.65	11.03		
Horizon		0.6	90.1		89.5		12.03	
MTD-2	**0.5**	**0.6**	**90.1**	**90.6**	**89.5**		**12.03**	0.85
Horizon		1.1	90.6		89.5		12.03	
Date (C14 cal)		1.1	92.06		90.96	13.74		
Date (U-Th)		1.1	92.20		91.1	14.07		
Horizon		1.1	95.80		94.70		15.86	
MTD-3	**0.6**	**1.1**	**95.8**	**96.4**	**94.7**		**15.86**	
Horizon		1.7	96.4		94.7		15.86	2.01
Horizon		1.7	101		99.3		18.14	
MTD-4	**1.1**	**1.7**	**101**	**102.1**	**99.3**		**18.14**	
Horizon		2.8	102.1		99.3		18.14	
Date (U-Th)		2.8	102.1		99.3	18.14		
Horizon		2.8	102.1		99.3		18.14	
MTD-5[a]	**0.77**	**2.8**	**102.1**	**102.87**	**99.3**		**18.14**	2.10
Horizon		3.57	103.2		99.63		18.30	
Date (C14 cal)		3.57	106		102.43	19.63		
Horizon		3.57	108.3		104.73		20.36	
MTD-6[a]	**0.54**	**3.57**	**108.3**	**108.84**	**104.73**		**20.36**	3.14
Horizon		4.11	108.9		104.79		20.38	
Date (C14 cal)		4.11	109.05		104.94	20.43		
Horizon		4.11	111.6		107.49		24.43	
MTD-7[a]	**0.54**	**4.11**	**111.6**	**112.14**	**107.49**		**24.43**	0.64
Horizon		4.65	112.2		107.55		24.53	
Date (C14 cal)		4.65	114.61		109.96	28.31		
Horizon		4.65	114.9		110.25		28.59	
MTD-8	**1.2**	**4.65**	**114.9**	**116.1**	**110.25**		**28.59**	
Horizon		5.85	116.1		110.25		28.59	
Horizon		5.85	117		111.15		29.46	
MTD-9[a]	**5.93**	**5.85**	**117**	**122.93**	**111.15**		**29.46**	
Horizon		11.78	124.9		113.12		31.37	1.03
Horizon		11.78	126		114.22		32.44	
MTD-10[a]	**2**	**11.78**	**126**	**128**	**114.22**		**32.44**	
Horizon		13.78	129		115.22		33.41	
Horizon		13.78	130.3		116.52		34.67	
MTD-11	**1.7**	**13.78**	**130.3**	**132**	**116.52**		**34.67**	
Horizon		15.48	132		116.52		34.67	
Horizon		15.48	131.62		116.14		34.30	
Date (C14 cal)		15.48	131.62		116.14	34.30		
Horizon		15.48	132.80		117.32		36.26	
MTD-12[a]	**3.13**	**15.48**	**132.8**	**135.93**	**117.32**		**36.26**	0.60
Horizon		18.61	137.5		118.89		38.86	
Date (U-Th)		18.61	139.27		120.66	41.80		
Date (C14 cal)		18.61	139.33		120.72	41.31		
Horizon		18.61	145.3		126.69		48.96	
MTD-13	**0.5**	**18.61**	**145.3**	**145.8**	**126.69**		**48.96**	
Horizon		19.11	145.8		126.69		48.96	
Horizon		19.11	146.5		127.39		49.86	
MTD-14	**3.2**	**19.11**	**146.5**	**149.7**	**127.39**		**49.86**	
Horizon		22.31	149.7		127.39		49.86	
Horizon		22.31	149.7		127.39		49.86	
MTD-15	**4.2**	**22.31**	**149.7**	**153.9**	**127.39**		**49.86**	
Horizon		26.51	153.9		127.39		49.86	
Horizon		26.51	155.5		128.99		51.91	0.78

Table 2. *(continued)*

	Thickness of added material (m)	Sum of added event thickness above (m)	Added material top, core depth (m)	Added material bottom, core depth (m)[b]	EFD (top) (m)	Dated horizons age (ka)	Event-free model ages (ka)	Event-free sedimentation rate (m/kyr)
MTD-16	**1.7**	**26.51**	**155.5**	**157.2**	**128.99**		**51.91**	
Horizon		28.21	157.2		128.99		51.91	
Horizon		28.21	157.2		128.99		51.91	
MTD-17	**0.7**	**28.21**	**157.2**	**157.9**	**128.99**		**51.91**	
Horizon		28.91	157.9		128.99		51.91	
Horizon		28.91	160.7		131.79		55.49	
MTD-18	**0.6**	**28.91**	**160.7**	**161.3**	**131.79**		**55.49**	
Horizon		29.51	161.3		131.79		55.49	
Horizon		29.51	161.4		131.89		55.62	
MTD-19	**0.7**	**29.51**	**161.4**	**162.1**	**131.89**		**55.62**	
Horizon		30.21	162.1		131.89		55.62	
Horizon		30.21	168.3		138.09		63.57	
MTD-20	**0.8**	**30.21**	**168.3**	**169.1**	138.09		**63.57**	
Horizon		31.01	169.1		138.09		63.57	
Date (U-Th)		31.01	174.52		143.51	70.51		
Horizon		31.01	179.5		148.49		75.88	
MTD-21	**0.6**	**31.01**	**179.5**	**180.1**	**148.49**		**75.88**	
Horizon		31.61	180.1		148.49		75.88	
Horizon		31.61	181.4		149.79		77.28	
MTD-22	**3.2**	**31.61**	**181.4**	**184.6**	**149.79**		**77.28**	
Horizon		34.81	184.6		149.79		77.28	0.93
Horizon		34.81	190.2		155.39		83.32	
MTD-23	**0.7**	**34.81**	**190.2**	**190.9**	**155.39**		**83.32**	
Horizon		35.51	190.9		155.39		83.32	
Horizon		35.51	191.4		155.89		83.86	
MTD-24	**0.6**	**35.51**	**191.4**	**192**	**155.89**		**83.86**	
Horizon		36.11	192		155.89		83.86	
Date (U-Th)		36.11	193.58		157.47	85.56		
Horizon		36.11	194		157.89		85.73	
MTD-25	**0.7**	**36.11**	**194**	**194.7**	**157.89**		**85.73**	
Horizon		36.81	194.7		157.89		85.73	
Horizon		36.81	195.3		158.49		85.97	
MTD-26	**0.5**	**36.81**	**195.3**	**195.8**	**158.49**		**85.97**	**2.50**
Horizon		37.31	195.8		158.49		85.97	
Horizon		37.31	198.3		160.99		86.97	
MTD-27	**0.5**	**37.31**	**198.3**	**198.8**	**160.99**		**86.97**	
Horizon		37.81	198.8		160.99		86.97	
Horizon		37.81	220.03		182.22		95.45	
Date (U-Th)		37.81	220.03		**182.22**	95.45		

Note. The entire thickness of the debrite-type units is removed, while for slumps two thirds (or more) are removed (see text). Every core depth has a corresponding EFD (event-free depth), on which the age model is based, and the inferred ages of the MTDs is the age at their corresponding EFD. Depths marked "Date (C14 cal)" are dated radiocarbon samples on organic matter from Kitagawa et al. (2017). Depths marked "Date (U-Th)" are dated uranium-thorium aragonite samples from Torfstein et al. (2015). Sample names for ages used in the event-free model are given in Table S1.
[a]Slumps for which not 100% of thickness was considered "added thickness" (see text). [b]For debrites refers to bottom of unit, for slumps refers to calculated depth of additional material.

and deposition of MTDs in the deep lake. This simultaneous significant erosion in the lake's margins and the formation of the thickest slumps in the depocenter attest to the instability of the area during major earthquakes.

4. The seismites show similar distribution during high and low lake stands. Nevertheless, major slumps appear in the depocenter during the lower stand MIS3 period (~50–31 ka).
5. The recurrence interval of thick MTD (>50 cm) in the depocenter is ~ 2,500 years, twice the recurrence interval at the marginal terraces. However, when all MTDs (>1 cm) are accounted for, the recurrence interval is ~100–300 years. These two values provide a range of recurrence intervals of seismites in the DSB.
6. Overall, there are up to an order of magnitude more abundant MTD layers in the deep-lake sequence of the Lisan Formation than at the lake's margin sections during the same time windows. This can be

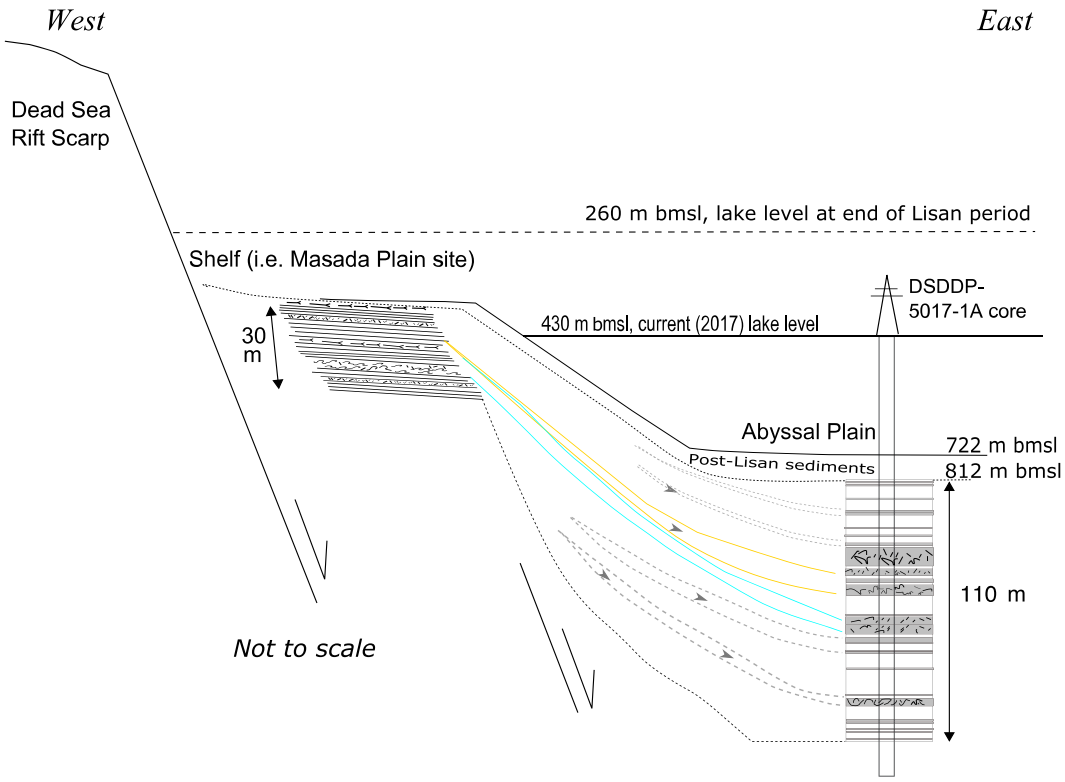

Figure 5. Schematic basin scenario. To the west, on the shelf, is situated a lake margin section (e.g., the Masada outcrop) with ~30 m of laminates, intraclast breccias (seismites), and some slumps. To the east, at the abyssal plain (DSDDP-5017-1-A core), lies a 110 m thick section, representing the late Pleistocene (last glacial) stratigraphic unit, the Lisan Formation. The deep-lake site includes ~28 m of laminates, 42 m of thick (>50 cm), and 40 m of thinner (<50 cm) homogenites, turbidites, breccias, and slumps (termed mass transport deposits, MTDs). The sites are correlated in detail in Figure 3 and in Table 1. In yellow is the correlation of a missing section at M1 site to thick MTDs in the core, and in blue is the correlation of a slump (the "convolute") at M1 with a thick slump in the core. The other slumps in the core may have originated further east of the currently outcropping lake margin sites on slope. Note that post-Lisan is ~90 m thick, not to scale here. No reflection data available on the subformation scale.

explained by the probability that slumps and turbulent sediment flows from many of the lake's slopes at all its sides may reach the depocenter, perhaps reflecting also the effects of smaller local earthquakes, and the possibility that lower earthquake intensity is needed for subsea sliding to initiate than near-shore brecciation and deformation.

7. Source of the MTDs

Structures of slumping and turbidite transport are notable in much of the core (Figure 2). Detrital beds >1 cm thick are also here considered transported deposits. They are ~10 times thicker than millimeter-scale *add* laminae and usually of disparate color. Similarly, Neugebauer et al. (2015) and Neugebauer et al. (2016) also considered graded detritus layers >1 cm as events that must be excluded from their varve-counting and comparison to outcrop sections in the Holocene portion of the core.

We propose that the source of the sediments in MTD beds (1 cm to ~790 cm thickness) in the DSDDP deep-lake Lisan core is transported sediments from the shelves or slope (Figure 5). In addition to the obvious transport structures (section 5.3), evidence for the formation of the slumps comes from the outcrops of the Lisan Formation at the marginal terraces (e.g., at Masada or Perazim Valley). Alsop and Marco (2012a, 2012b, 2013) interpreted the asymmetric geometry of slump sheets documented at the exposed outcrops of the Lisan Formation at Perazim Valley (Figure 1) as reflecting dominant transport toward the depocenter down negligible (<1°) subaqueous slopes. The preservation of continuous bedding suggests that the transport was along short distances and limited to the close vicinity of the shelf. We therefore conclude that the folded slumps in the core were only transported short distances from the

core site. However, many units (e.g., turbidites, breccias) showing no original laminae are notable in much of the DSDDP core (Figure 2). These beds are termed debrites (1 cm to 420 cm thickness), and we suggest that they were transported from the shelves or slopes at the circumlakes margins (Figure 5). Evidence for recent "transport of sediment" process is provided by slumping scars documented in the bathymetry, shoreline morphology, and exposed shelf edge (Kagan & Lensky, 2017; Lensky et al., 2014).

Based on the above mentioned considerations, transport mostly initiated at the shelf edge or slope but occurred also possibly at the deep basin. The location of the shelf edge of Lake Lisan is unknown. The near-shore core DSDDP-5017-3 drilled off Ein Gedi Spa (Figure 1) comprises a ~65 m thick sequence of the Lisan Formation sediments. The description of this core is available at the ICDP data repository (http://dead-sea.icdp-online.org/). The Lisan Formation thickness in the shallow core is thicker than the ~25–40 m thickness of the Lisan outcrops but is significantly thinner than the 110 m thick section at the abyssal plains. This near-shore core shows much less prominent slump structures than the deep core but includes many thick and thin debrites. This core has yet to be studied or dated, but the thickness difference and lithology suggest to us that it includes significant quantities of transported sediments.

Slumps and debrites are ubiquitous within seismically active regions (e.g., Goldfinger et al., 2007; Strasser et al., 2013). In the seismically active DSB we argue that the deformation is associated with the seismic activity along the DST. As mentioned here above, at the margins of the Dead Sea historical earthquakes have been correlated with sediment deformation. The Dead Sea's predecessor, Lake Lisan, shows lake margin slumps and debrites (breccias) with direct association with faulting. Niemi and Ben Avraham (1994) identified in seismic reflection data one large shallow slump at the northern end of the Dead Sea and argued that it was triggered by the M_L 6.25 Jericho earthquake of 11 July 1927. The setting of the DSB supports seismically induced mass transport and as a working hypothesis will be considered as such.

8. Paleoseismological Implications

Based on the continuous sedimentary section in the core, in contrast to the incomplete temporal coverage of the outcrops along the western basin margins, we suggest that we now have a more complete paleoseismic record of the entire DSB for the last glacial period when Lake Lisan reached its highest stands and filled the entire tectonic basin.

An important observation of our study is the difference between the earthquake records of Perazim, Masada, and Beit Ha'Arava sites (Figure 3) that possibly reflects the location of the sites in relation to the major nearby faults. Because of the attenuation, earthquakes that rupture segments south of the basin might not trigger seismite formation in Beit Ha'Arava, and earthquakes that rupture the Jordan Valley segment might not trigger seismites in the PZ1 site. We attribute the large number of seismites in the drill core to its central location, where seismites record earthquakes on any fault around the basin. In terms of hazard, the central part of the basin experienced moderate to large earthquake ($M > 6.5$) every ~1,100 years. The mean recurrence interval of ~1,100 translates to M~6.5 based on the combined records from microseismicity, historical accounts, and seismites (Figure 6). Earthquake clusters of several millennia are typical of individual sites but may not be apparent if basin-wide activity is considered. These inferences predict that if on-fault records are recovered by paleoseismic investigations on different segments of the Dead Sea Fault System, each of them will exhibit temporal clusters, but the clusters will be diachronous across sites. Off-fault records are more complete than on-fault records because they do not depend on our ability to recognize all the possible active fault strands, but in turn they do not provide accurate information on location of the earthquake source.

Overall, this unprecedented chronology of seismic activity in Lake Lisan provides a framework of earthquake activity in the vicinity of the late Pleistocene DSB during conditions of high-lake stand that could be compared with that of the Holocene period when the lake receded and occupied only a small part of the tectonic basin. While the paleoseismic records of the exposed or drilled terraces at the lake's margins are well established (e.g., Kagan et al., 2011; Ken-Tor et al., 2001, 2001; Migowski et al., 2004), this comparison waits for the completion of the description of the seismic record of the deep core during the time interval of the Holocene.

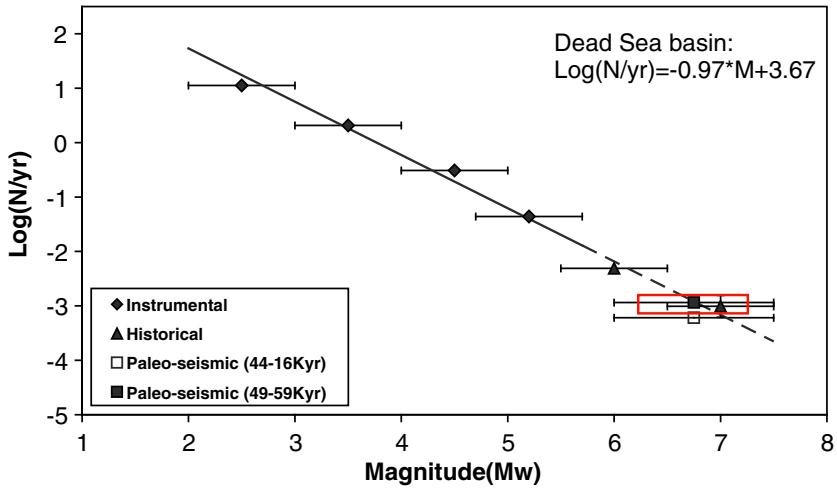

Figure 6. The mean recurrence interval (*y* axis) of ~1,100 years seen in this study (marked here by red box) corresponds to *M*~6.5, based on the combined records from microseismicity, historical accounts, and seismites, according to the magnitude-frequency curve of Hamiel et al. (2009).

9. Conclusions

1. The Lisan Fm. lake margin sections at Perazim (PZ1 section), Masada (M1 section), and Beit Ha'Arava (BA1 section) are 23–38-m thick, of which 5–10% are seismites. The different numbers of seismites are interpreted as a combined effect of the different earthquakes that affected these localities and missing sedimentary intervals (hiatuses) in the individual sections (e.g., at ~49–43.5 and ~40–31 ka, in PZ1 and M1, respectively). Since these missing segments of the specific sedimentary sections appear in the other sites, it was possible to produce basin-wide integrated earthquake record for the DSB that reflects the regional seismic activity associated with the DST. The following points illustrate the major observations and conclusions of this paper:
2. Integrating the data from the three exposed marginal sites (PZ1, M1, and BA1), the minimum number of seismites during the Lisan interval is 49. The average recurrence interval of the seismites in the DSB, as represented by the three studied sites, is ~1,100 years. Considering only the 31 to 17.5 ka Upper Member of the Lisan Formation (the White Cliff) at the M1 section (Masada), the recurrence interval of the seismites is ~1,200 years, very similar to the average recurrence time during the entire Lisan time period. Similarly, in other complete intervals, for Upper Member at Perazim, and the middle and lower members of Beit Ha'Arava, a similar recurrence interval of ~ 1,000 years is calculated. These recurrence intervals are within the ranges that have been calculated for *M*~6.5–7 by Begin et al. (2005) and by Hamiel et al. (2009) (Figure 6).
3. The previous scenario of ~10 kyr of clustering of seismites (i.e., earthquakes) that alternate with ~10 kyr of quiescence in the Lisan period (Marco et al., 1996) requires reconsideration in light of the new chronological data and basin-wide stratigraphic correlation (e.g., Haase-Schramm et al., 2004; Torfstein, Goldstein, Kagan, et al., 2013) that revealed several significant hiatuses in the individual sections. Here we establish an integrated basin-wide record of seismic events that fills the gaps caused by the hiatuses.
4. Mass transport deposits (from cm-scale up to almost 8 m thick) comprise ~75% of the deep lake Lisan Fm. thickness. Pronounced seismites in the marginal terraces coincide with those of significant slumps in the depocenter, e.g., the convolute unit at Masada is correlated with a ~ 4 m slump in the depocenter. This indicates "intrabasin" response to major seismic events at the vicinity of the Dead Sea.
5. The recurrence interval of thick MTD (>50 cm) in the depocenter is ~2,500 years, twice the recurrence interval than at the marginal terraces; however, when all MTDs (>1 cm) are accounted for, there is a mean recurrence interval of ~100–300 years. These two values provide a range of recurrence interval of seismites in the entire DSB.
6. In all, there are up to an order of magnitude more abundant MTD layers in the deep-lake Lisan Formation than during the same time period in the lake margin sections. This difference can be explained by the probability that slumps and turbulent sediment flows from many of the lake's slopes may reach the

depocenter, perhaps from smaller local earthquakes, and the possibility that lower earthquake intensity is needed for subsea sliding to initiate than near-shore brecciation and deformation.

7. Earthquake clusters of several millennia are typical of individual sites but may not be apparent if basin-wide activity is considered. This may suggest that if on-fault records are recovered by paleoseismic investigations on different segments of the DST, each of them will exhibit temporal clusters, but the clusters will be diachroneous across sites.

The Dead Sea deep-lake core provides a first look into Dead Sea MTDs accumulated at the lake basin floor. Comparison of the last glacial period Lake Lisan MTDs with lake margin earthquake-triggered breccias and slumps allows an intrabasin study of deformed and transported lake sediment paleoseismology.

Acknowledgments

We thank the Editor and two anonymous reviewers for helping to significantly improve the paper. The Dead Sea drilling project was carried out by ICDP (International Continental Scientific Drilling Programs). We thank all people who participated in the drilling operation, the opening, and the description of the cores at GFZ-Potsdam. We wish to thank Markus Schwab, Achim Brauer, and Ina Neugebauer who organized the opening and sampling campaigns. We sincerely thank Adi Torfstein, Ina Neugebauer, and Daniel Palchan for fruitful discussions on the sedimentology and chronology of the ICDP cores and the marginal terraces of the Lisan Formation. The core raw data are available from http://deadsea.icdp-online.org/. The DSDDP cores are now stored at the International Core Repository at the University of Bremen. The study was supported by the ISF Excellence Center of the Israel Science Foundation (ISF) grants 1736/11 and 1436/14 to S. M.

References

Adams, J. (1996). Paleoseismology in Canada: A dozen years of progress. *Journal of Geophysical Research*, *101*(B3), 6193–6207. https://doi.org/10.1029/95JB01817

Agnon, A. (2014). Pre-instrumental earthquakes along the Dead Sea rift. In *Dead Sea Transform fault system: Reviews* (pp. 207–261). Netherlands: Springer.

Agnon, A., Migowski, C., & Marco, S. (2006). Intraclast breccia layers in laminated sequences: Recorders of paleo-earthquakes. In Y. Enzel, A. Agnon, & M. Stein (Eds.), *New frontiers in Dead Sea paleoenvironmental research*, *Geological Society of America Special Paper* (Vol. 401, pp. 195–214). https://doi.org/10.1130/2006.2401(13)

Alsop, G. I., & Marco, S. (2011). Soft-sediment deformation within seismogenic slumps of the Dead Sea basin. *Journal of Structural Geology*, *33*(4), 433–457. https://doi.org/10.1016/j.jsg.2011.02.003

Alsop, G. I., & Marco, S. (2012a). Tsunami and seiche-triggered deformation of offshore sediments. *Sedimentary Geology*, *261–262*, 90–107.

Alsop, G. I., & Marco, S. (2012b). A large-scale radial pattern of seismogenic slumping towards the Dead Sea basin. *Journal of the Geological Society*, *169*(1), 99–110. https://doi.org/10.1144/0016-76492011-032

Alsop, G. I., & Marco, S. (2014). Fold and fabric relationships in temporally and spatially evolving slump systems: A multi-cell flow model. *Journal of Structural Geology*, *63*, 27–49. https://doi.org/10.1016/j.jsg.2014.02.007

Alsop, G. I., & Marco, S. (2013). Seismogenic slump folds formed by gravity-driven tectonics down a negligible subaqueous slope. *Tectonophysics*, *605*, 48–69.

Ambraseys, N. (2009). *Earthquakes in the Mediterranean and Middle East: A multidisciplinary study of seismicity up to 1900*. Cambridge, UK: Cambridge University Press. https://doi.org/10.1017/CBO9781139195430

Avşar, U., Jónsson, S., Avşar, Ö., & Schmidt, S. (2016). Earthquake-induced soft-sediment deformations and seismically amplified erosion rates recorded in varved sediments of Köyceğiz Lake (SW Turkey). *Journal of Geophysical Research: Solid Earth*, *121*, 4767–4779. https://doi.org/10.1002/2016JB012820

Bartov, Y., Enzel, Y., Porat, N., & Stein, M. (2007). Evolution of the late Pleistocene–Holocene Dead Sea basin from sequence statigraphy of fan deltas and lake-level reconstruction. *Journal of Sedimentary Research*, *77*(9), 680–692. https://doi.org/10.2110/jsr.2007.070

Bartov, Y., Goldstein, S. L., Stein, M., & Enzel, Y. (2003). Catastrophic arid episodes in the Eastern Mediterranean linked with the North Atlantic Heinrich events. *Geology*, *31*(5), 439–442.

Begin, B. Z., Steinberg, D. M., Ichinose, G. A., & Marco, S. (2005). A 40,000 years unchanging of the seismic regime in the Dead Sea rift. *Geology*, *33*(4), 257–260. https://doi.org/10.1130/G21115.1

Ben-Menahem, A. (1991). Four thousand years of seismicity along the Dead Sea rift. *Journal of Geophysical Research*, *96*(B12), 20,195–20,216. https://doi.org/10.1029/91JB01936

Blais-Stevens, A., & Clague, J. J. (2001). Paleoseismic signature in late Holocene sediment cores from Saanich Inlet, British Columbia. *Marine Geology*, *175*(1-4), 131–148. https://doi.org/10.1016/S0025-3227(01)00132-3

Blumberg, S., Lamy, F., Arz, H. W., Echtler, H. P., Wiedicke, M., Haug, G. H., & Oncken, O. (2008). Turbiditic trench deposits at the south-Chilean active margin: A Pleistocene–Holocene record of climate and tectonics. *Earth and Planetary Science Letters*, *268*(3-4), 526–539. https://doi.org/10.1016/j.epsl.2008.02.007

Chapron, E., Beck, C., Pourchet, M., & Deconinck, J. F. (1999). 1822 earthquake-triggered homogenite in Lake Le Bourget (NW Alps). *Terra Nova*, *11*(2-3), 86–92. https://doi.org/10.1046/j.1365-3121.1999.00230.x

Freund, R., Zak, I., & Garfunke, Z. (1968). Age and rate of sinistral movement along Dead Sea rift. *Nature*, *220*(5164), 253–255. https://doi.org/10.1038/220253a0

Garfunkel, Z. (1981). Internal structure of the Dead-Sea leaky transform (rift) in relation to plate kinematics. *Tectonophysics*, *80*(1-4), 81–108. https://doi.org/10.1016/0040-1951(81)90143-8

Goldfinger, C., Nelson, C. H., & Johnson, J. E. (2003). Holocene earthquake records from the Cascadia subduction zone and northern San Andreas fault based on precise dating of offshore turbidites. *Annual Review of Earth and Planetary Sciences*, *31*(1), 555–577. https://doi.org/10.1146/annurev.earth.31.100901.141246

Goldfinger, C., Morey, A. E., Nelson, C. H., Gutiérrez-Pastor, J., Johnson, J. E., Karabanov, E., … Party, S. S. (2007). Rupture lengths and temporal history of significant earthquakes on the offshore and north coast segments of the northern San Andreas fault based on turbidite stratigraphy. *Earth and Planetary Science Letters*, *254*(1-2), 9–27. https://doi.org/10.1016/j.epsl.2006.11.017

Haase-Schramm, A., Goldstein, S. L., & Stein, M. (2004). U-Th dating of Lake Lisan (late Pleistocene Dead Sea) aragonite and implications for glacial East Mediterranean climate change. *Geochimica et Cosmochimica Acta*, *68*(5), 985–1005. https://doi.org/10.1016/j.gca.2003.07.016

Haliva-Cohen, A., Stein, M., Goldstein, S. L., Sandler, A., & Starinsky, A. (2012). Sources and transport routes of fine detritus material to the late Quaternary Dead Sea basin. *Quaternary Science Reviews*, *50*, 55–70. https://doi.org/10.1016/j.quascirev.2012.06.014

Hamiel, Y., Amit, R., Begin, Z. B., Marco, S., Katz, O., Salamon, A., … Porat, N. (2009). The seismicity along the Dead Sea fault during the last 60,000 years. *Seismological Society of America Bulletin*, *99*, 2020–2026. https://doi.org/10.1785/0120080218

Kagan, Y. Y., & Jackson, D. D. (1991). Long-term earthquake clustering. *Geophysical Journal International*, *104*(1), 117–134. https://doi.org/10.1111/j.1365-246X.1991.tb02498.x

Kagan, E. J., & Lensky, N. (2017). Shelf-edge exposure at the receding Dead Sea: Syn-deposition landsliding. Geological Society of Israel Annual Meeting. Mitzpe Ramon.

Kagan, E., Stein, M., Agnon, A., & Neumann, F. (2011). Intrabasin paleoearthquake and quiescence correlation of the late Holocene Dead Sea. *Journal of Geophysical Research*, *116*, B04311. https://doi.org/10.1029/2010JB007452

Ken-Tor, R., Agnon, A., Enzel, Y., Stein, M., Marco, S., & Negendank, J. F. W. (2001). High-resolution geological record of historic earthquakes in the Dead Sea basin. *Journal of Geophysical Research*, *106*(B2), 2221–2234. https://doi.org/10.1029/2000JB900313

Kitagawa, H., Stein, M., Goldstein, S. L., Nakamura, T., & Lazar, B. (2017). Radiocarbon chronology of the DSDDP core at the deepest floor of the Dead Sea. *Radiocarbon*, *59*(02), 383–394. https://doi.org/10.1017/RDC.2016.120

Lazar, B., Sivan, O., Yechieli, Y., Levy, E. J., Antler, G., Gavrieli, I., & Stein, M. (2014). Long-term freshening of the Dead Sea brine revealed by porewater Cl^- and in ICDP Dead Sea deep-drill. *Earth and Planetary Science Letters*, *400*, 94–101. https://doi.org/10.1016/j.epsl.2014.03.019

Le Beon, M., Klinger, Y., Amrat, A. Q., Agnon, A., Dorbath, L., Baer, G., … Mayyas, O. (2008). Slip rate and locking depth from GPS profiles across the southern Dead Sea Transform. *Journal of Geophysical Research*, *113*, B11403. https://doi.org/10.1029/2007JB005280

Lensky N. G., Calvo R., Sade A. R., Gavrieli I., Katz O., Hall J., Enzel Y. & Mushkin A. (2014). The scarred slopes of the Dead Sea—Evidence for intensive subsea landsliding, Israel Geological Society Annual Meeting, Ein Bokek.

Levy, E. J., Stein, M., Lazar, B., Gavrieli, I., Yechieli, Y., & Sivan, O. (2017). Pore fluids in Dead Sea sediment core reveal linear response of lake chemistry to global climate changes. *Geology*, *45*(4), 315–318. https://doi.org/10.1130/G38685.1

Machlus, M., Enzel, Y., Goldstein, S. L., Marco, S., & Stein, M. (2000). Reconstructing low levels of Lake Lisan by correlating fan-delta and lacustrine deposits. *Quaternary International*, *73-4*, 137–144.

Marco, S., & Agnon, A. (1995). Prehistoric earthquake deformations near Masada, Dead Sea graben. *Geology*, *23*(8), 695–698. https://doi.org/10.1130/0091-7613(1995)023%3C0695:PEDNMD%3E2.3.CO;2

Marco, S., & Agnon, A. (2005). High-resolution stratigraphy reveals repeated earthquake faulting in the Masada fault zone, Dead Sea Transform. *Tectonophysics*, *408*(1-4), 101–112. https://doi.org/10.1016/j.tecto.2005.05.036

Marco, S., & Klinger, Y. (2014). Review of on-fault palaeoseismic studies along the Dead Sea fault. In *Dead Sea Transform fault system: Reviews* (pp. 183–205). Netherlands: Springer.

Marco, S., Stein, M., Agnon, A., & Ron, H. (1996). Long-term earthquake clustering: A 50,000-year paleoseismic record in the Dead Sea graben. *Journal of Geophysical Research*, *101*(B3), 6179–6191. https://doi.org/10.1029/95JB01587

Masson, F., Hamiel, Y., Agnon, A., Klinger, Y., & Deprez, A. (2015). Variable behavior of the Dead Sea fault along the southern Arava segment from GPS measurements. *Comptes Rendus Geoscience*, *347*(4), 161–169. https://doi.org/10.1016/j.crte.2014.11.001

McCalpin, J. P. (2009). In R. Dmowska & J. R. Holton (Eds.), *Paleoseismology*, *International Geophysical Series* (Vol. 62, p. 613). San Diego, CA: Academic Press.

Migowski, C., Agnon, A., Bookman, R., Negendank, J. F. W., & Stein, M. (2004). Recurrence pattern of Holocene earthquakes along the Dead Sea Transform revealed by varve-counting and radiocarbon dating of lacustrine sediments. *Earth and Planetary Science Letters*, *222*(1), 301–314. https://doi.org/10.1016/j.epsl.2004.02.015

Moernaut, J., Daele, M. V., Heirman, K., Fontijn, K., Strasser, M., Pino, M., … De Batist, M. (2014). Lacustrine turbidites as a tool for quantitative earthquake reconstruction: New evidence for a variable rupture mode in south central Chile. *Journal of Geophysical Research: Solid Earth*, *119*, 1607–1633. https://doi.org/10.1002/2013JB010738

Morey, A. E., Goldfinger, C., Briles, C. E., Gavin, D. G., Colombaroli, D., & Kusler, J. E. (2013). Are great Cascadia earthquakes recorded in the sedimentary records from small forearc lakes? *Natural Hazards and Earth System Sciences*, *13*(10), 2441–2463. https://doi.org/10.5194/nhess-13-2441-2013

Mulder, T., & Alexander, J. (2001). The physical character of subaqueous sedimentary density flows and their deposits. *Sedimentology*, *48*(2), 269–299. https://doi.org/10.1046/j.1365-3091.2001.00360.x

Neev, D., & Emery, K. O. (1967). The Dead Sea—Depositional processes and environments of evaporites. *Israel Geological Survey Bulletin*, *41*, 1–147.

Neugebauer, I., Brauer, A., Schwab, M. J., Waldmann, N. D., Enzel, Y., Kitagawa, H., … Ariztegui, D. (2014). Lithology of the long sediment record recovered by the ICDP Dead Sea Deep Drilling Project (DSDDP). *Quaternary Science Reviews*, *102*, 149–165. https://doi.org/10.1016/j.quascirev.2014.08.013

Neugebauer, I., Brauer, A., Schwab, M. J., Dulski, P., Frank, U., Hadzhiivanova, E., … Waldmann, N. D. (2015). Evidences for centennial dry periods at ~ 3300 and~ 2800 cal. yr BP from micro-facies analyses of the Dead Sea sediments. *The Holocene*, *25*(8), 1358–1371. https://doi.org/10.1177/0959683615584208

Neugebauer, I., Schwab, M. J., Waldmann, N. D., Tjallingii, R., Frank, U., Hadzhiivanova, E., … Brauer, A. (2016). Hydroclimatic variability in the Levant during the early last glacial (~ 117–75 ka) derived from micro-facies analyses of deep Dead Sea sediments. *Climate of the Past*, *12*(1), 75–90. https://doi.org/10.5194/cp-12-75-2016

Niemi, T. M., & Ben-Avraham, Z. (1994). Evidence for Jericho earthquakes from slumped sediments of the Jordan River delta in the Dead Sea. *Geology*, *22*(5), 395–398.

Salamon, A., Hofstetter, A., Garfunkel, Z., & Ron, H. (2003). Seismotectonics of the Sinai subplate—The eastern Mediterranean region. *Geophysical Journal International*, *155*(1), 149–173. https://doi.org/10.1046/j.1365-246X.2003.02017.x

Schnellmann, M., Anselmetti, F. S., Giardini, D., & Mckenzie, J. A. (2006). 15,000 years of mass-movement history in Lake Lucerne: Implications for seismic and tsunami hazards. *Eclogae Geologicae Helvetiae*, *99*(3), 409–428. https://doi.org/10.1007/s00015-006-1196-7

Schramm, A., Stein, M., & Goldstein, S. L. (2000). Calibration of the ^{14}C time scale to$>$ 40 ka by ^{234}U–^{230}Th dating of Lake Lisan sediments (last glacial Dead Sea). *Earth and Planetary Science Letters*, *175*(1-2), 27–40. https://doi.org/10.1016/S0012-821X(99)00279-4

Schwab, M. J., Werner, P., Dulski, P., McGee, E., Nowaczyk, N. R., Bertrand, S., & Leroy, S. A. (2009). Palaeolimnology of Lake Sapanca and identification of historic earthquake signals, northern Anatolian fault zone (Turkey). *Quaternary Science Reviews*, *28*(11-12), 991–1005. https://doi.org/10.1016/j.quascirev.2009.02.018

Stein, M. (2001). The sedimentary and geochemical record of Neogene-Quaternary water bodies in the Dead Sea Basin-inferences for the regional paleoclimatic history. *Journal of Paleolimnology*, *26*(3), 271–282.

Stein, M. (2011). Paleo-earthquakes chronometry in the late Quaternary Dead Sea: Israel. *Journal of Earth Science*, *58*, 264–282.

Stein, M. (2014). The evolution of Neogene-Quaternary water-bodies in the Dead Sea Rift Valley. In Z. Garfunkel, et al. (Eds.), *Dead Sea Transform fault system: Reviews*, *Modern Approaches in Solid Earth Sciences 6* (Vol. 279, pp. 279–316). Dordrecht, Netherlands: Springer Science. https://doi.org/10.1007/978-94-017-8872-4_10

Stein, M., & Goldstein, S. L. (2006). Dating the late Pleistocene Dead Sea sedimentary record by U-Th and radiocarbon methods: Approaches and applications. In Y. Enzel, A. Agnon, & M. Stein (Eds.), *New frontiers in Dead Sea paleoenvironmental research*, *Geological Society of America Special Paper 401* (pp. 141–154). https://doi.org/10.1130/2006.2401(09)

Stein, M., Ben-Avraham, Z., & Goldstein, S. L. (2011). Dead Sea cores: A window into past climate and seismicity. *Eos*, *453*.

Stein, M., Lazar, B., Torfstein, A., & Goldstein, S. L. (2017). In Y. Enzel & O. Bar Yosef (Eds.), *Chronologies of late Quaternary coral reefs and lake sediments from the Red Sea and Dead Sea Rift Valley. Quaternary of the Levant*. Cambridge, UK: Cambridge University Press.

Strasser, M., Monecke, K., Schnellmann, M., & Anselmetti, F. S. (2013). Lake sediments as natural seismographs: A compiled record of late Quaternary earthquakes in central Switzerland and its implication for Alpine deformation. *Sedimentology*, *60*(1), 319–341. https://doi.org/10.1111/sed.12003

Torfstein, A., Goldstein, S. L., Kagan, E. J., & Stein, M. (2013). Integrated multi-site U–Th chronology of the last glacial Lake Lisan. *Geochimica et Cosmochimica Acta*, *104*, 210–231. https://doi.org/10.1016/j.gca.2012.11.003

Torfstein, A., Goldstein, S. L., Stein, M., & Enzel, Y. (2013). Impacts of abrupt climate changes in the Levant from last glacial Dead Sea levels. *Quaternary Science Reviews*, *69*, 1–7. https://doi.org/10.1016/j.quascirev.2013.02.015

Torfstein, A., Goldstein, S. L., Kushnir, Y., Enzel, Y., Haug, G., & Stein, M. (2015). Dead Sea drawdown and monsoonal impacts in the Levant during the last interglacial. *Earth and Planetary Science Letters*, *412*, 235–244. https://doi.org/10.1016/j.epsl.2014.12.013

Waldmann, N., Starinsky, A., & Stein, M. (2007). Primary carbonates and Ca-chloride brines as monitors of a paleo-hydrological regime in the Dead Sea basin. *Quaternary Science Reviews*, *26*(17–18), 2219–2228.

Wilhelm, B., Nomade, J., Crouzet, C., Litty, C., Sabatier, P., Belle, S., … Anselmetti, F. S. (2016). Quantified sensitivity of small lake sediments to record historic earthquakes: Implications for paleoseismology. *Journal of Geophysical Research: Earth Surface*, *121*, 2–16. https://doi.org/10.1002/2015JF003644